Cellular and Molecular Life Sciences (2025) 82:135
https://doi.org/10.1007/s00018-025-05665-1

ORIGINAL ARTICLE

Genome-wide profiling and functional characterization of circular RNAs in neural development and injury: insights from a rat model research

Jian Yang[1,2] · Nana Jin[2,3] · Shuqiang Zhang[2] · Ya Tan[2] · Zhifeng Chen[2] · Xiaoli Huang[3] · Guicai Li[2] · Bin Yu[2] · Jianhua Shi[3] · Xiaosong Gu[2] · Zhiming Cui[4] · Lian Xu[2,3]

Received: 10 August 2024 / Revised: 12 November 2024 / Accepted: 17 March 2025
© The Author(s) 2025

Abstract

Circular RNAs (circRNAs) have re-emerged as promising gene regulators in various physiological and pathological conditions. However, the expression patterns of circRNAs in the developing spinal cord of mammals and the comprehensive distribution of circRNAs across different tissues remain poorly understood. In this study, rats were used as the model organism. We conducted a comprehensive analysis of 15 RNA-Seq datasets comprising 217 rat samples and developed a web-based resource, CiRNat, to facilitate access to these data. We identified 15,251 credible circRNAs and validated them through experimental approaches. Notably, we observed two significant time points for circRNA increase during spinal cord development, approximately at embryonic day 14 (E14d) and postnatal week 4 (P4w). Analysis of circRNA expression in various rat tissues revealed higher expression levels in central nervous system tissues compared to peripheral nervous system tissues and other tissues. Furthermore, some highly abundant circRNAs exhibited tissue- and species-specific expression patterns and differed from their cognate linear RNAs, such as those derived from *Gigyf2*. Integrating polysome profiling and bioinformatic predictions suggested potential functions of certain circRNAs as miRNA sponges and translational templates. Collectively, this study provides the first comprehensive landscape of circRNAs in the developing spinal cord, offering an important resource and new insights for future exploration of functional circRNAs in central nervous system development and related diseases.

Keywords CircRNA · Neurogenesis · Tissue-specific expression · Gene regulation · Nervous system · Translational potential

Abbreviations

circRNAs	Circular RNAs
CNS	Central nervous system

Jian Yang, Nana Jin and Shuqiang Zhang contributed equally to this work.

✉ Xiaosong Gu
nervegu@ntu.edu.cn

✉ Zhiming Cui
zhimingcuispine@163.com

✉ Lian Xu
xulian@ntu.edu.cn

[1] Department of Neurosurgery, People's Hospital of Deyang City, Sichuan Clinical Research Center for Neurological Diseases, Deyang, Sichuan, China

[2] Key Laboratory of Neuroregeneration of Jiangsu and Ministry of Education, Co-Innovation Center of Neuroregeneration, NMPA Key Laboratory for Research and Evaluation of Tissue Engineering Technology Products, Nantong University, Nantong, Jiangsu, China

[3] Institute for Translational Neuroscience, The Second Affiliated Hospital of Nantong University, Nantong University, Nantong, Jiangsu, China

[4] Department of Spine Surgery, The Second Affiliated Hospital of Nantong University, Nantong University, Nantong, Jiangsu, China

Published online: 01 April 2025

PNS	Peripheral nervous system
qPCR	Quantitative Real-time PCR
RNase R	Ribonuclease R
BSJ	Back-Splicing junction
RNA-Seq	RNA sequencing
ORF	Open reading frame
IRES	Internal ribosome entry site
m6A	N6-methyladenosine
miRNAs	MicroRNAs
RBPs	RNA-binding proteins
SNC	Sciatic nerve crush
SCI	Spinal cord injury
DRG	Dorsal root ganglion

Introduction

Circular RNAs (circRNAs), a class of single-stranded RNA molecules prevalent in eukaryotes, have re-emerged as key regulators in gene expression, participating in various biological processes, such as neural development, neuropsychiatric diseases, and tumorigenesis [1–4]. Studies have shown that circRNAs can exert their regulatory functions through mechanisms like binding to miRNAs, interacting with RNA-binding proteins, and serving as templates for translation [5–7]. CircRNAs are typically produced by back-splicing, a process that creates covalently closed loops without a 3′ polyA tail, making them resistant to exonuclease digestion [8]. Advances in deep sequencing, particularly ribosome-depleted RNA sequencing (total RNA-Seq) and RNase R-treated transcriptomes, have enable the identification of numerous circRNAs across different cell lines and tissues in humans and mice [9–11].

Despite their low expression levels, circRNAs show distinct and dynamic expression patterns across different cell types and tissues, particularly in the central nervous system (CNS) where they are enriched in synapses and neuropil [10, 11]. Studies have characterized circRNAs in the developing brain (hippocampus) and retina at several developmental stages, demonstrating consistent up-regulation during mouse development [11–13]. However, circRNAs in earlier stages of CNS development remain largely unexplored, especially in the spinal cord, a critical CNS component that mediates sensory and motor functions. Spinal cord injury (SCI) can result in severe and often irreversible impairment of motor and sensory functions, underscoring the need to understand circRNA roles in spinal cord development and injury [14]. While circRNA dysregulation in SCI has been investigated [15], a genome-wide characterization of circRNAs specific to the developing spinal cord remains unaddressed.

Our study aims to fill this gap by providing a comprehensive landscape of circRNAs during spinal cord development and following injury in rats. We re-analyzed a long-term time-series dataset of total RNA sequencing from developing and injured spinal cords, as well as relevant public datasets, to examine the dynamic expression of circRNAs. Our analysis includes 217 samples from 15 RNA-Seq datasets of rats with longer read lengths (≥ 75 bp), which enhances detection accuracy and enables us to capture a broader range of circRNAs. For comparison, we also re-analyzed 94 samples from 7 RNA-Seq datasets of mice, allowing us to identify species-specific circRNA expression patterns. Additionally, we developed a user-friendly web application (CiRNat), to make this extensive dataset accessible to the scientific community.

This work provides an essential resource for understanding the roles of circRNAs in neural development and injury. By revealing the spatiotemporal expression patterns of circRNAs during spinal cord development, this study offers new insights into how circRNAs may contribute to neural development and response to injury. Our findings not only advance the field of neurobiology but also open new avenues for research into potential therapeutic targets for CNS injuries and neurodegenerative diseases.

Materials and methods

Animals and tissue preparation

Sprague Dawley (SD) rats were obtained from the Experimental Animal Center of Nantong University. All animal experiments were performed following the guidelines of the Nantong University Institutional Animal Care and Use Committee. For experiments of circRNAs expression during the spinal cord development, the spinal cord was dissected from rats at the ages of E11d, E18d, P1d, P2w and P8w. Rats at the age of eight weeks were used to dissect other tissues, including the cortex, hippocampus, spinal cord, heart, liver, and kidney.

RNase R treatment

Total RNA was isolated from the spinal cord using TRIZOL reagent (Thermo Fisher Scientific, USA) according to the manufacturer's protocol. RNA purity and concentration were assessed using a Nanodrop spectrophotometer (Thermo Fisher Scientific, USA). For RNase R treatment, 1 μg of total RNA was either treated with 0 units (control) or 20 units of RNase R (Vazyme, China) in a reaction buffer consisting of 200 mM Tris–HCl (pH 8.0), 1 M KCl, and 0.1 mM $MgCl_2$. The treatment was conducted at 37 ℃ for 1 h, followed by RNase R inactivation at 65 ℃ for 20 min. RNase R-treated RNA and untreated control RNA were reverse transcribed to complementary DNA (cDNA) using HiScript III RT SuperMix for qPCR (Vazyme, China) according to

the manufacturer's standard protocol. The resulting cDNA was stored at −20 ℃ until use.

Validation of circRNAs

To validate the presence of circRNAs, the cDNA from the RNA with RNase treatment was amplified in a 20 µL reaction containing 1 µL of cDNA, 0.3 µM of each primer, and 10 µL of 2 × Rapid Taq Plus Master Mix (Vazyme, China). The PCR cycling conditions were as follows: initial denaturation at 95 °C for 2 min, followed by 32 cycles of 98 °C for 10 s, 58 °C for 30 s, and 68 °C for 10 s, with a final extension at 68 °C for 5 min. The divergent primer pairs flanking the back-splice site were designed using Prime3 online primer design web tool (http://bioinfo.ut.ee/primer3-0.4.0/primer3/) and were shown in Supplementary file 5: Table S4. The PCR products were subjected to 1.5% agarose gel electrophoresis at 100 V for 45 min. The PCR products were extracted from the agarose gel using FastPure Gel DNA Extraction Mini Kit (Vazyme, China). Sanger sequencing (Azenta, China) was further used to verified the extracted circRNAs. All experiments were performed with three biological replicates to ensure reliability and reproducibility of the results.

qPCR

To assess the relative expression of circRNA candidates, quantitative Real-time PCR (qPCR) assays were performed using TaqPro Universal SYBR qPCR Master Mix (Vazyme, China) and conducted with the CFX96 Real-Time PCR System (Bio-Rad, USA). The primers were shown in Supplementary file 5: Table S4. The expression of candidates was calculated relative to the housekeeping gene *Gapdh*. All quantitative PCR reactions were conducted in triplicate. Equal amplification efficiencies for target and reference transcripts were confirmed using melting curve analysis.

Validation of circRNAs

To assess the relative expression of circRNA candidates, quantitative Real-time PCR (qPCR) assays were performed using TaqPro Universal SYBR qPCR Master Mix (Vazyme) and conducted with the CFX96 Real-Time PCR System (Bio-Rad). *Gapdh* was amplified as a control. The expression of candidates was calculated relative to the housekeeping gene. To validate the presence of circRNAs, PCR products were subjected to agarose gel electrophoresis. The purified PCR products excised from the agarose gel are sent to Azenta for Sanger sequencing. The divergent primers flanking the back-splicing site were designed and listed in Supplementary file 5: Table S4. All experiments were performed with three biological replicates to ensure reliability and reproducibility of the results.

Quality-check and pre-filtering of Ribo-Zero RNA-seq datasets

Raw RNA-seq Fastq files of analyzed public datasets were downloaded from the NCBI SRA database (accession were recorded in Supplementary file 2: Table S1 and Supplementary file 3: Table S2). FastQC was used for quality checks and Fastp v0.23.2 [16] was used for trimming adapters and low-quality reads filtering. The newly released rat reference genome (mRatBN7.2/rn7) and annotation were used and downloaded from the Ensembl website (https://ftp.ensembl.org/pub/release-109/fasta/rattus_norvegicus/). The mouse reference genome (GRCm39) and annotation were downloaded from the GENCODE database (vM27). We extracted rRNA reference sequences from the annotation file and aligned clean reads against rRNA sequences using Bowtie2 v2.3 [17] to estimate the percent of rRNAs.

Identification and quantification of circular RNAs as well as linear RNAs

The raw sequencing data of rRNA-depleted RNA-Seq from developing rat spinal cord were retrieved from our previous study [18]. Firstly, the trimming tool, Fastp, was used to remove low-quality reads and subsequent to the CIRCexplorer3 pipeline [19] using the default parameters, including genome mapping, extraction of unmapped reads, and identification and quantification of circular RNAs and their cognate linear RNAs. Circular RNAs supported by at least two back-splicing reads (BSJ read count ≥ 2) in at least two samples from a timepoint were kept for the study. The same pipeline was applied to other total RNA-seq and polysome profiling datasets.

Comparison of circular RNAs with the public database

CircAtlas [20] is a database that provides a comprehensive circRNAs across multiple species, including rat. To compare with rat circRNAs deposited in this database (circAtlas v3.0), we firstly downloaded bed formatted file of rat circular RNAs (Rn6) and converted into the new reference (Rn7) coordinates using liftOver command-line tool. The consistent circRNAs were counted when their back-splicing junction was the same.

Developmental- and injured-regulated circRNA analysis

To detect developmental- or injured-regulated circRNAs in rat spinal cord, we employed the maSigPro package [21] to

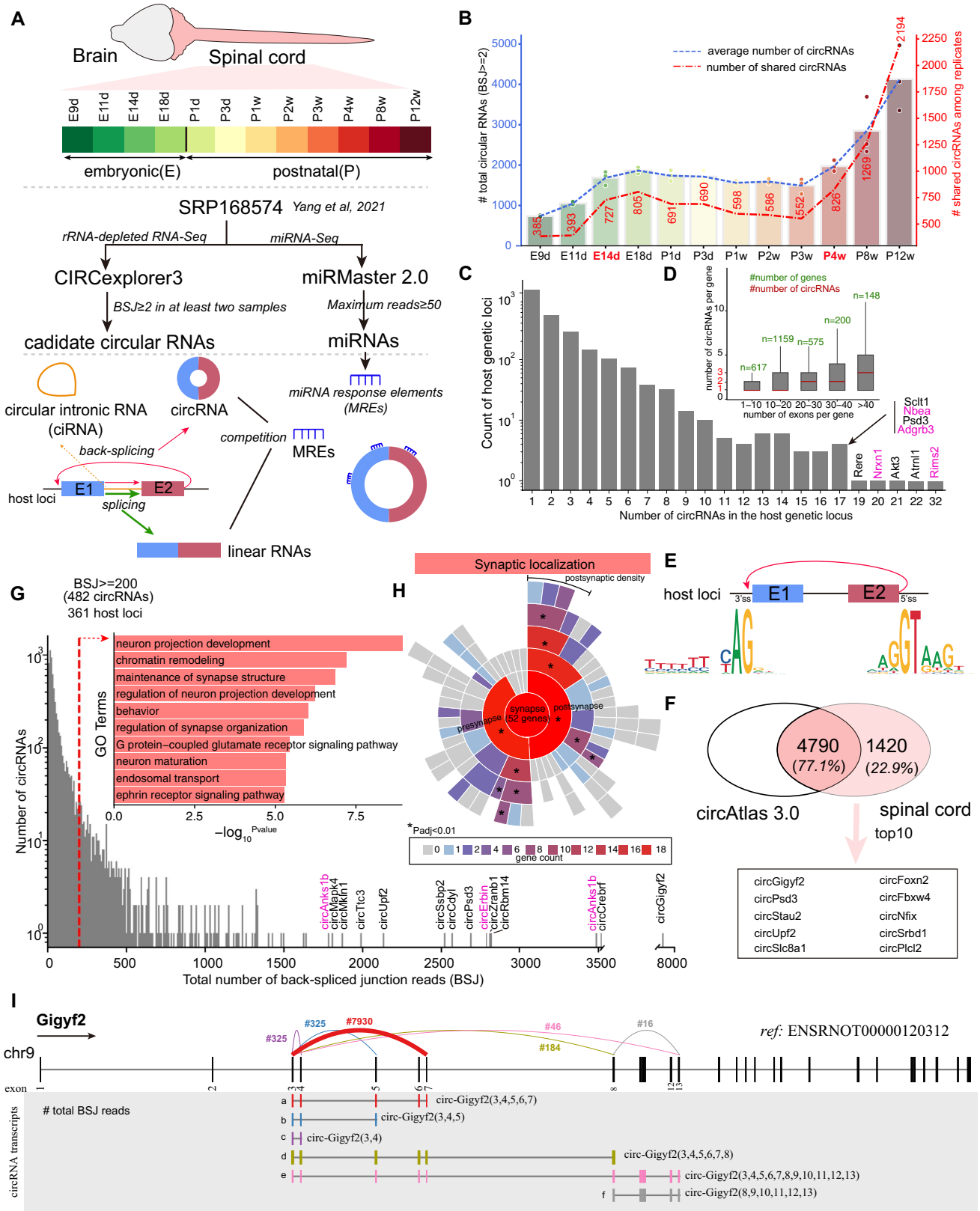
A
Brain
Spinal cord
E9d E11d E14d E18d P1d P3d P1w P2w P3w P4w P8w P12w
embryonic(E)
postnatal(P)
SRP168574 Yang et al, 2021
rRNA-depleted RNA-Seq
miRNA-Seq
CIRCexplorer3
miRMaster 2.0
BSJ≥2 in at least two samples
Maximum reads≥50
cadidate circular RNAs
miRNAs
circular intronic RNA (ciRNA)
circRNA
miRNA response elements (MREs)
competition
MREs
back-splicing
host loci
E1
E2
splicing
linear RNAs
B
average number of circRNAs
number of shared circRNAs
total circular RNAs (BSJ>=2)
shared circRNAs among replicates
385
393
727
805
691
690
598
586
552
826
1269
2194
C
Count of host genetic loci
Number of circRNAs in the host genetic locus
D
#number of genes
#number of circRNAs
number of circRNAs per gene
number of exons per gene
n=617
n=1159
n=575
n=200
n=148
Sclt1
Nbea
Psd3
Adgrb3
Rere
Nrxn1
Akt3
Atrnl1
Rims2
E
host loci
E1
E2
3'ss
5'ss
F
4790 (77.1%)
1420 (22.9%)
circAtlas 3.0
spinal cord
top10
circGigyf2
circPsd3
circStau2
circUpf2
circSlc8a1
circFoxn2
circFbxw4
circNfix
circSrbd1
circPlcl2
G
BSJ>=200
(482 circRNAs)
361 host loci
Number of circRNAs
GO Terms
neuron projection development
chromatin remodeling
maintenance of synapse structure
regulation of neuron projection development
behavior
regulation of synapse organization
G protein–coupled glutamate receptor signaling pathway
neuron maturation
endosomal transport
ephrin receptor signaling pathway
−log10 Pvalue
Total number of back-spliced junction reads (BSJ)
circAnks1b
circMapk4
circMkln1
circTtc3
circUpf2
circSsbp2
circCdyl
circPsd3
circErbin
circZranb1
circRbm14
circAnks1b
circCrebrf
circGigyf2
H
Synaptic localization
postsynaptic density
synapse (52 genes)
postsynapse
presynapse
*Padj<0.01
gene count
I
Gigyf2
chr9
exon
ref: ENSRNOT00000120312
#325
#7930
#46
#16
#184
total BSJ reads
circRNA transcripts
a circ-Gigyf2(3,4,5,6,7)
b circ-Gigyf2(3,4,5)
c circ-Gigyf2(3,4)
d circ-Gigyf2(3,4,5,6,7,8)
e circ-Gigyf2(3,4,5,6,7,8,9,10,11,12,13)
f circ-Gigyf2(8,9,10,11,12,13)

◂**Fig. 1** Genome-wide characterization of circRNAs in the developing rat spinal cord. **A** The schema of the analysis. **B** The number of the average (left y-axis) and shared circRNAs among replicates (right y-axis) in each developmental time point. **C** The summary of circRNA number generated by per host loci. **D** The summary of the relationship between circRNA number and exon number. **E** The motif pattern of circRNAs detected in developing spinal cord. **F** The overlap of circRNAs identified in developing spinal cord and circAtlas 3.0. **G** The high abundance of circRNAs (total BSJ read count ≥ 200) and functional enrichment of host loci. **H** Enrichment of synaptic location geneset for host loci generating a high abundance of circRNAs (total BSJ count ≥ 200). **I** Six expressed circRNAs generated from *Gigyf2*. Colorful link lines indicated BSJ from different circRNAs and number labelled text indicated the total BSJ count in developing spinal cord. Number in the brackets indicated included candidate exons in circRNAs

identify differentially expressed circRNAs along the developmental or injured time-points.

Identification of conserved circRNAs between rat and mouse

Conserved circRNAs were defined if the exon(s) that formed the BSJ are orthologous to the mouse exon(s) that also formed the BSJ. Briefly, exon(s) forming the BSJ of circRNAs was parsed from GTF-formatted annotation files of rat and mouse (downloaded from GenCode, M27 version) and obtained orthologous exon(s) in mouse using the liftOver tool. Bedtools intersect module with the parameter "-loj" was used to obtain matched exon(s) in mouse and then the result was manually checked.

miRNA quantification and target prediction

miRNA-Seq dataset of developing spinal cord were retrieved from our previous study [18]. Pre-processing, identification and quantification of miRNAs were performed using the web-based tool, miRMaster [22] (https://ccb-compute.cs.uni-saarland.de/mirmaster2/). miRNAs with the maximum number of reads greater than 50 in at least two replicates were kept. To predict candidate miRNAs targeting pseudo-circRNAs, the first 20 nt at beginning of the sequence was extracted and then concatenated behind the last 20 nt into a pseudo circRNA. Single-exon derived circRNAs were also used to predict miRNA targets. Miranda [23] (option: −en −10 −sc 140), PITA [24] (ΔΔG = −10) and TargetScan [25] (type: m8 or m8:1a) were employed to predict. miRNA-targets supported by three tools were kept.

Prediction cORF, IRES and m6A sites

The cORF pipeline [6] was employed to predict circRNA ORFs. IRESfinder [26] was employed to detect candidate IRES sequences with the parameter, model 2 (window size: 174; step size: 50). The standalone SRAMP program [27] was employed to predict m6A sites.

Statistical analysis

A two-sided unpaired t-test was performed to compare the expression levels of circRNAs between CNS tissues and non-CNS tissues. A one-way ANOVA was used to assess whether there were differences in circRNA expression levels across various CNS tissues. The statistical analysis was conducted using the R programming, with a significance threshold set at $p < 0.05$.

Results

Genome-wide characterization of circular RNAs in the developing rat spinal cord

To characterize genome-wide and dynamic circular RNAs in the developing spinal cord, we analyzed our long-term time-series of rRNA-depleted RNA-Seq dataset ranging from the early embryonic stage (embryonic 9 days, E9d) to the adult (12 weeks postnatal, P12w) with a total of twelve timepoints [18] (Fig. 1A and Supplementary file 2: Table S1). We employed a robust and accurate pipeline for the identification and quantification of both circular RNAs and linear RNAs, CIRCExplore3 [19], and used the newly released rat genome (mRatBN7.2) as the reference. Both circular exonic RNAs (circRNAs) and circular intronic RNAs (ciRNAs) could be detected by the CIRCExplore3. Here we only focused on circRNAs due to a low abundance of ciRNAs (most ciRNAs with BSJ read count ≤ 2, Supplementary file 1: Fig. S1). To screen the high-confidence of circRNAs, those with at least two back-splicing junction (BSJ) reads in at least two samples from a developmental timepoint were kept for the downstream analysis. A total of 6,210 circRNA candidates generating from 2696 loci met the criterion and most were flanked by the canonical splicing motif, AG-GT (Fig. 1E). We also compared with rat circular RNAs deposited in the circAtlas database [20]. About 77.1% (4790 out of 6210) of the total circular RNAs were annotated in the circAtlas database to date based on the genomic coordinates of BSJ (Fig. 1F). Among the unannotated circRNAs, the top10 abundant circRNAs included circular transcripts generated from host loci of *Gigyf2*, *Psd3* and *Slc8a1* (Fig. 1F). Analysis of the number of circular RNAs in each time point, we found the smallest number at early embryonic stage (E9d-E11d), and increased at E14d and then small fluctuation until P3w, and gradually increased from the P4w (Fig. 1B). Most host loci generated a small number (< 10) of circRNAs but nine host loci could generate

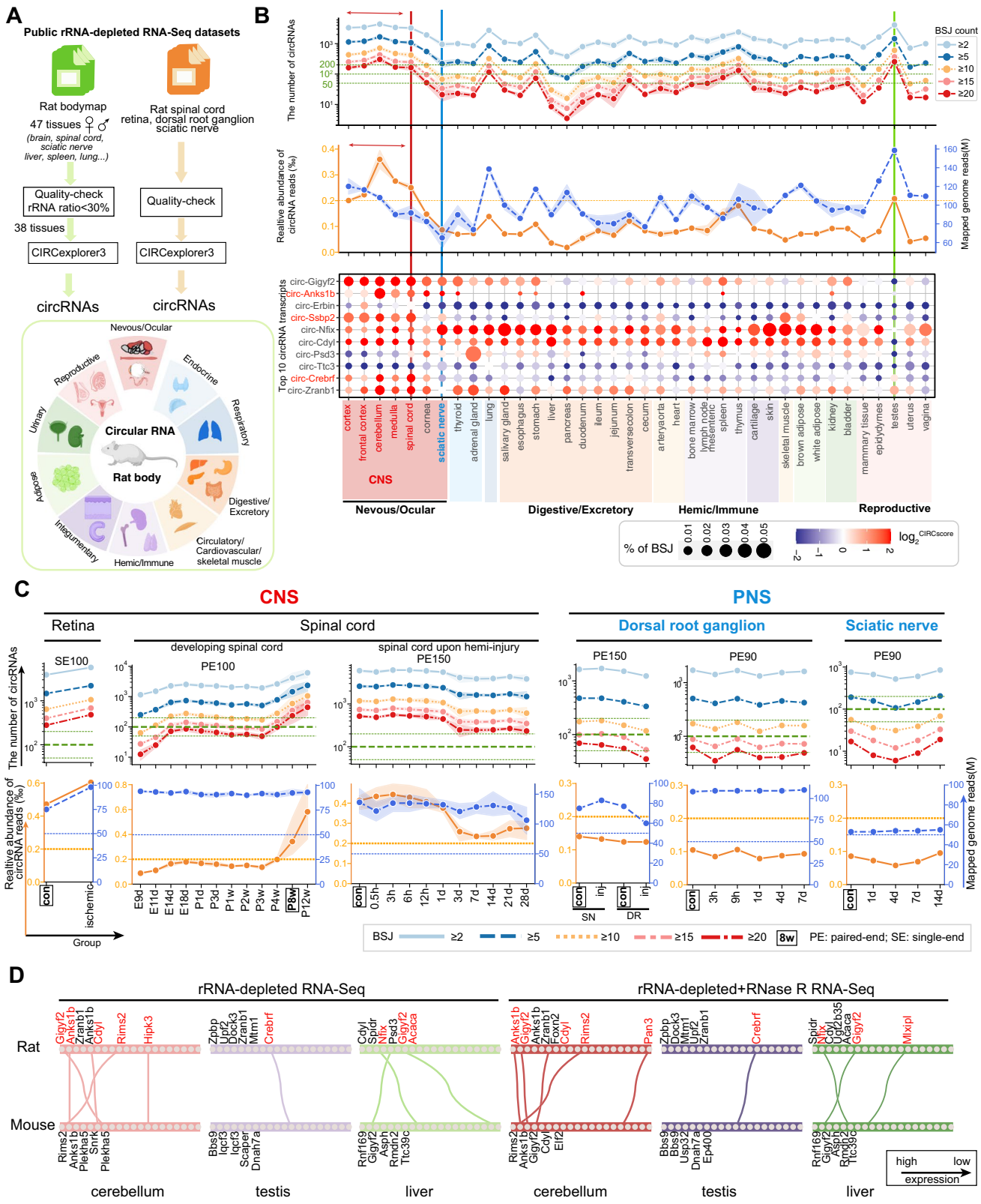

more than 17 circRNA transcripts (also known as a hotspot which contains multiple circRNAs originating from the same loci [28]), including four synapse-related genes, *Rims2*, *Nrxn1*, *Nbea*, and *Adgrb3* (Fig. 1C). We also noticed that 248 out of 1283 loci (19.32%) with at least two circRNAs generated one major circRNA (defined with at least

◂**Fig. 2** Highly abundant circRNAs in CNS but not in PNS. **A** The schema of analysis workflow and was created with BioRender.com. **B** The number and abundance of the circRNAs in the rat body. The upper panel showed the number of circRNAs under different thresholds. The middle panel showed the ratio of circRNAs (orange) and uniquely mapped reads (blue). The bottom panel showed the top 10 abundant circRNAs. Circle colors indicate CIRCscore and sizes indicate the relative expression abundance respectively. **C** The circular number and abundance in rat retina, spinal cord, DRG and sciatic nerve in other studies. **D** The top 20 abundant circRNAs in three tissues from two species using rRNA-depleted or further with RNase R treatment. Text labelled showed host loci generating the top 5 circRNAs as well as conserved circRNAs in between mouse and rat. Link lines between rat circRNAs and mouse circRNAs indicated orthologous pairs

fivefold of the expression of the second circRNA transcript level), especially *Gigyf2* (generating six circRNAs (designed as a–e) and the 'a' transcript was the major circRNA, Fig. 1I and Supplementary file 1: Fig. S2). Consistent with the previous report [29], the increased number of circRNAs was observed along with the increased exon number per gene (Fig. 1D). We next investigated highly abundant circRNAs in the spinal cord. Functional enrichment analysis showed that host loci generating circRNAs with a total of BSJ read count ≥ 200 were significantly enriched in terms of "neuron projection development" and "maintenance of synapse structure" (Fig. 1G). Further synaptic localization annotation and enrichment analysis showed that 52 out of 361 host loci were located at synapse and the most were located at postsynaptic density (Fig. 1H), which was consistent with a previous report in the mouse brain [11]. Taken together, these results displayed and characterized circular RNAs in the developing rat spinal cord.

Highly abundant circRNAs in CNS but not in PNS

It is commonly acknowledged that the brain harbors a significantly higher abundance of circular RNAs (circRNAs) in comparison to other tissues, such as the liver, lung, and heart. While previous studies have delved into the analysis of circRNAs in 11 tissues (brain and various non-nervous system tissues) of developing and aging rats at different life stages (2 w, 6 w, 21 w, and 105 w) [30, 31], these investigations remain incomplete and somewhat understated due to the relatively short length of sequencing reads (~ 50 bp). Moreover, there is still a notable gap in the systematic comparison of circular RNAs between the central nervous system (consisting of the brain, spinal cord, and retina) and the peripheral nervous system (PNS, encompassing structures like the dorsal root ganglion (DRG) and sciatic nerve), as well as other diverse tissues in rats.

Fortunately, Krause et al. have recently constructed an extensive gene expression atlas encompassing four preclinical species, among which is the rat, covering up to 47 tissues (88 samples, encompassing female and male samples of the brain, spinal cord, retina, and sciatic nerve) across 12 major organ systems [32]. This endeavor was achieved using an rRNA-depleted and paired-end sequencing strategy with a read length of 75 bp (PE75), thereby providing an invaluable resource for exploring circRNAs throughout the rat's body, particularly within the nervous system. Hence, we next investigated circRNAs in rat diverse organ system using this valuable resource as well as previously independent public related datasets, including retina, spinal cord, DRG and sciatic nerve after injury [33, 34] (Fig. 2A). We first performed quality-check of samples from the rat body dataset and discarded those samples with a high percent of rRNA (> 30%) and finally kept 72 samples from 38 tissues (*e.g.*, brain, spinal cord, sciatic nerve) with at least 50 million (M) uniquely mapped reads for the analysis (Fig. 2A and 2B, Supplementary file 3: Table S2). It showed the highest number and abundance (estimated by the total BSJ read count) of circRNAs in CNS tissues (cortex, cerebellum, medulla, spinal cord etc.), with the testes showing the next highest level compared with other tissues, including sciatic nerve (Fig. 2B). Of the different brain regions, circRNAs in cerebellum showed the most abundance (Fig. 2B), which is also consistent with the observation in mouse [10] (*e.g.*, 3046 circRNAs in cerebellum, 2353 circRNAs in cortex using the same pipeline, Supplementary file 1: Fig. S3). We also confirmed circRNA abundance in other public datasets from brain, retina and spinal cord, and other PNS tissues (DRG and sciatic nerve). As observed, the number and abundance of circRNAs in adult retina and spinal cord were greater than that in adult PNS tissues (*e.g.*, highly expressed circRNAs (BSJ read count ≥ 20 in at least a sample (without replicate) or two replicates)) was greater than 130, while that in PNS tissues was less than 70, Fig. 2C). Interestingly, in our analyzed datasets, we noticed that global abundance of total circRNAs in retina after ischemic stroke injury (12 h) was increased while global abundance of total circRNAs in spinal cord was obviously decreased after 3 days post hemi-transection injury (Fig. 2C). One example is a circRNA generated from the exon 4 of rat *Zranb1* loci (ENSRNOT00000023257) that showed a markedly increased expression in the injured rat retina induced by glaucoma [35]. However, we found expression of most circRNAs generated from *Zranb1* loci in rat spinal cord upon SCI were decreased (Supplementary file 1: Fig. S4), suggesting different expression patterns of circRNAs in injury response of distinct neural tissues. Taken together, by integrating available rat total RNA sequencing datasets and a unified analysis workflow, we showed that the highest abundance of circRNAs in CNS tissues, specifically in the cerebellum, compared with that in PNS tissues and other organs.

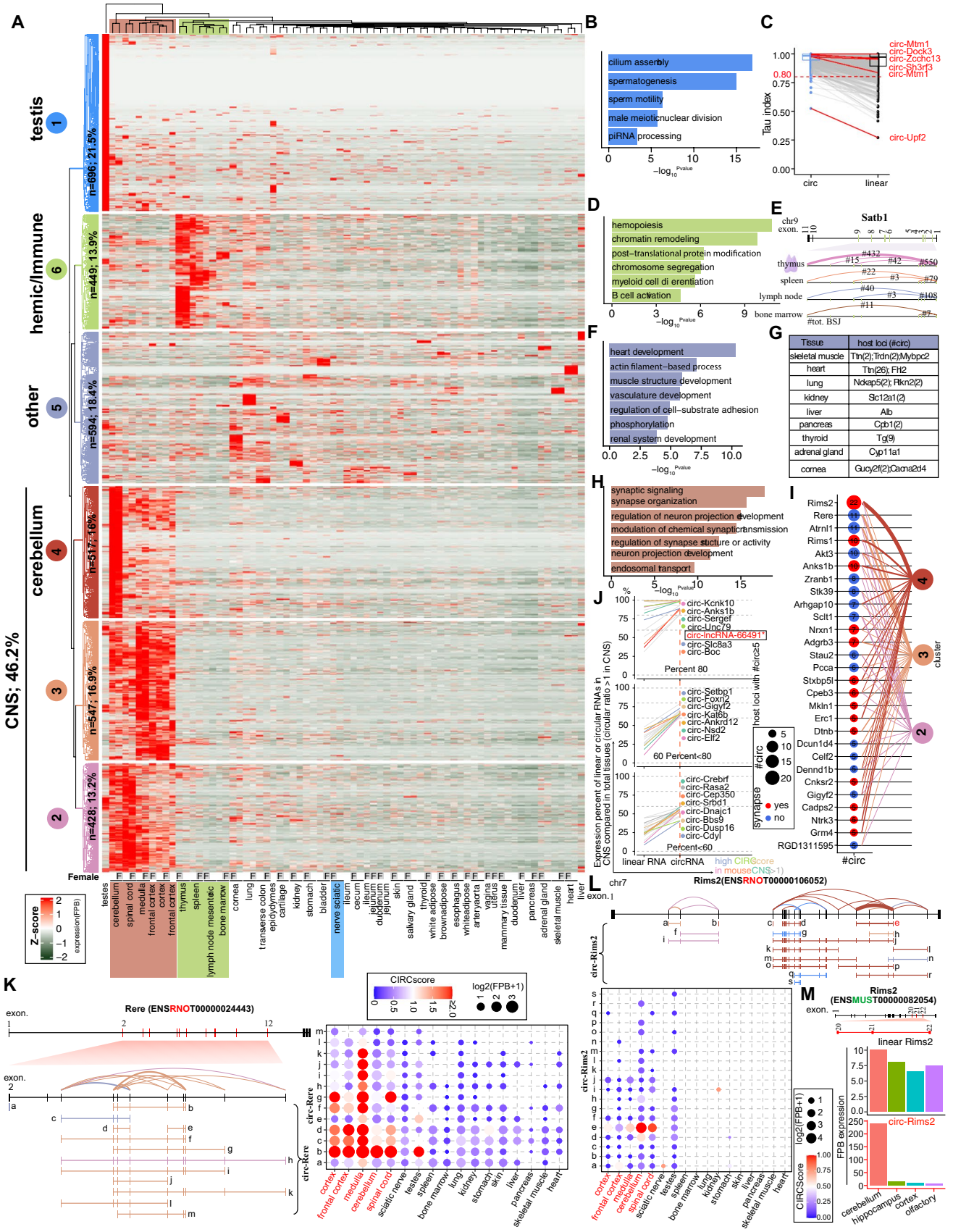
A
testis
hemic/Immune
other
cerebellum
CNS; 46.2%
n=696; 21.5%
n=449; 13.9%
n=594; 18.4%
n=517; 16%
n=547; 16.9%
n=428; 13.2%
Female
Z-score
expression(FPB)
testes
cerebellum
spinal cord
medulla
frontal cortex
cortex
frontal cortex
thymus
spleen
lymph node mesenteric
bone marrow
cornea
lung
transverse colon
epididymes
cartilage
kidney
stomach
bladder
nerve sciatic
ileum
cecum
ileum
duodenum
jejunum
skin
salivary gland
thyroid
white adipose
brownadipose
esophagus
whiteadipose
arteryaorta
uterus
mammary tissue
duodenum
liver
pancreas
adrenal gland
skeletal muscle
heart
liver
B
cilium assembly
spermatogenesis
sperm motility
male meiotic nuclear division
piRNA processing
−log10 Pvalue
C
Tau index
circ
linear
circ-Mtm1
circ-Dock3
circ-Zcchc13
circ-Sh3rf3
circ-Mtm1
circ-Upf2
D
hemopoiesis
chromatin remodeling
post−translational protein modification
chromosome segregation
myeloid cell di erentiation
B cell activation
E
Satb1
chr9
exon.
thymus
spleen
lymph node
bone marrow
#tot. BSJ
F
heart development
actin filament−based process
muscle structure development
vasculature development
regulation of cell−substrate adhesion
phosphorylation
renal system development
G
Tissue | host loci (#circ)
skeletal muscle | Ttn(2);Trdn(2);Mybpc2
heart | Ttn(26); Fhl2
lung | Ndrap5(2); Rbm20(2)
kidney | Slc12a1(2)
liver | Alb
pancreas | Cpb1(2)
thyroid | Tg(9)
adrenal gland | Cyp11a1
cornea | Gucy2f(2);Cacna2d4
H
synaptic signaling
synapse organization
regulation of neuron projection development
modulation of chemical synaptic transmission
regulation of synapse structure or activity
neuron projection development
endosomal transport
I
Rims2
Rere
Atrnl1
Rims1
Akt3
Anks1b
Zranb1
Stk39
Arhgap10
Sclt1
Nrxn1
Adgrb3
Stau2
Pcca
Stxbp5l
Cpeb3
Mkln1
Erc1
Dtnb
Dcun1d4
Celf2
Dennd1b
Cnksr2
Gigyf2
Cadps2
Ntrk3
Grm4
RGD1311595
#circ
cluster
J
Expression percent of linear or circular RNAs in CNS compared in total tissues (circular ratio >1 in CNS)
circ-Kcnk10
circ-Anks1b
circ-Sergef
circ-Unc79
circ-lncRNA-66491*
circ-Slc8a3
circ-Boc
Percent 80
circ-Setbp1
circ-Foxn2
circ-Gigyf2
circ-Kat6b
circ-Ankrd12
circ-Nsd2
circ-Elf2
60 Percent<80
circ-Crebrf
circ-Rasa2
circ-Cep350
circ-Srbd1
circ-Dnajc1
circ-Bbs9
circ-Dusp16
circ-Cdyl
Percent<60
linear RNA
circRNA
host loci with #circ≥5
#circ
synapse
yes
no
high CIRCscore in mouseCNS(>1)
K
Rere (ENSRNOT00000024443)
exon.
circ-Rere
CIRCscore
log2(FPB+1)
cortex
frontal cortex
medulla
cerebellum
spinal cord
sciatic nerve
testes
spleen
bone marrow
lung
kidney
stomach
skin
liver
pancreas
skeletal muscle
heart
L
Rims2(ENSRNOT00000106052)
chr7
exon.
circ-Rims2
M
Rims2
(ENSMUST00000082054)
linear Rims2
circ-Rims2
FPB expression
cerebellum
hippocampus
cortex
olfactory

◂**Fig. 3** CNS-enriched circRNAs in adult rat tissues. **A** The expression patterns of high abundant circRNAs in diverse rat tissues. **B** The top functional enrichment of host loci generating circRNAs in cluster 1. **C** Tissue-specificity of linear and circular forms of cluster 1 host loci. Red text indicated CIRCscore greater than 1. **D** The top functional enrichment of host loci generating circRNAs in cluster 6. **E** An example of immune-enriched circRNAs derived from *Satb1*. **F** The top functional enrichment of host loci generating circRNAs in cluster 5. **G** Examples of tissue-specific loci. Number in the bracket indicted the number of tissue-specific circRNAs. **H** The top functional enrichment of host loci generating circRNAs in CNS-enriched clusters 2, 3, and 4. **I** The loci generate multiple circRNAs and cluster information. Line width represents the number of circRNAs. **J** The expression percent of linear RNAs and circRNAs. Colorful lines and dots indicated that a higher CIRCscore in both rat and mouse orthologous circRNAs except a circRNA generating from a lncRNA (red star). **K** CircRNAs generated from Rere and expression in major rat tissues. **L** CircRNAs generated from *Rims2* and expression in major rat tissues. **M** A conserved *Rims2*-dervied circRNA ortholog in mouse and its expression in different brain regions

In addition, circRNAs generated from genetic loci of *Gigyf2*, *Anks1b*, *Erbin*, *Ssbp2*, *Nfix*, *Cdyl*, *Psd3*, *Ttc3*, *Crebrf*, and *Zranb1*, ranked the top 10 of the abundance in the rat body dataset based on the total BSJ read count (Fig. 2B). Except for a circRNA generated from a CNS-specific gene (*Anks1b*), others top abundant circRNAs were broadly expressed in most tissues (e.g., circ-*Gigyf2*). Of these, circRNAs generated from *Gigyf2*, *Nfix*, *Cdyl* and *Zranb1* showed a higher expression than that for cognate linear transcripts with a CIRCscore > 1 (namely $FPB_{circ} > FPB_{linear}$, Fig. 2B) in most tissues. We noticed other two circRNAs (circ-*Ssbp2* and circ-*Crebrf*) showed an obvious higher CIRCscore in CNS tissues than that in other tissues. Unlike in rat, the most abundance of circRNAs in mouse include circRNAs generated from host loci, *Rims2*, *Cdr1os*, *Anks1b*, *Gigyf2*, *Elf2*, using a total RNA-Seq dataset from mouse 14 tissues [9] (Supplementary file 1: Fig. S5). We then checked this phenomenon using another public dataset from the same study [28] and found that the most abundant circRNAs differed in tissues between rat and mouse, specifically in testis (the top 20 were shown in Fig. 2D and Supplementary file 1: Fig. S6). For example, a *Zpbp*-derived circRNA ranked the top in both the total RNA Sequencing and RNase R treatment datasets from rat testis, but a *Bbs9*-dervied circRNA ranked the top in both the total RNA Sequencing and RNase R treatment datasets from mouse testis (Fig. 2D). The well-explored circular *Cdr1as* (also known as ciRS-7), originating from a long non-coding RNA locus (Cdr1os), is the most abundant in human and mouse brains [5, 36]. However, we noticed that *Cdr1os* loci was absent in the rat genome annotation. Thus, given diverged expression and sequence in circRNAs across species, it still requires a comprehensive understanding of circRNA species in rat, especially in tissues, development and diseases.

CNS-enriched circRNAs in Rat

Next, we focused on circRNA transcripts with a high abundance (BSJ read count ≥ 5) in a tissue identified from the rat body dataset and performed unsupervised clustering analysis. A total of 3231 circRNAs were clustered into six clusters and most circRNAs showed CNS- (46.2%), testis- (21.5%) and hemic/immune- (13.9%) enriched (Fig. 3A). Functional enrichment analysis of host genes generating those circRNAs in each cluster was performed. Host loci in cluster 1 were enriched in terms related with spermatogenesis (Fig. 3B). Analysis of tissue-specificity of circular and their cognate linear transcripts showed that most were testis-specific (tau index > 0.8) and the specificity of circular transcripts was greater than that in linear form (Fig. 3C). Six circRNA transcripts showed a higher expression than that in cognate linear transcripts, including circRNAs originating from *Dock3* and *Mtm1*. Host loci (e.g., *Satb1*) generating circRNAs in cluster 6 were most enriched in terms related with immune, including myeloid cell differentiation (Fig. 3D and 3E). Host loci generating circRNAs in cluster 5 were enriched in tissue/organ development, including heart development, vasculature development and renal development (Fig. 3F). These loci included some tissue-specific genes, and most circRNAs originating from those loci were almost tissue-specific, such as *Alb* in liver and *Ttn* in heart (Fig. 3G). *Ttn* (Titin), encoding a giant protein, consisting of 349 exons in rat, generated 33 expressed circRNAs with 29 heart-specific and 2 skeletal muscle-specific (Fig. 3G and Supplementary file 1: Fig. S7). Of *Ttn*-derived circRNAs, the circRNA (*Ttn*-circ(143,144)) showed a similar abundance in between heart and skeletal muscle with a total BSJ read count of 105, respectively (Supplementary file 1: Fig. S7).

Host loci generating circRNAs in CNS-enriched clusters were most enriched in terms of nervous system development, including synaptic signaling and neuron projection development (Fig. 3H). Analysis of loci that generated multiple circRNA transcripts (≥ 5) showed 14 synapse-related genes, including *Rims1*, *Rims2* and *Anks1b* (Fig. 3I). Of 22 *Rims2*-derived circRNAs, most showed a higher expression in cerebellum than that in other CNS tissues. In general, most loci generate a major circRNA transcript. For example, *Rims2*-circ(20, 21, 22, 23) (namely e transcript in Fig. 3L) was the most abundance and showed a greater expression than the linear form. The orthologous exons formed BSJ of that circRNA in mouse (namely *Rims2*-circ(20, 21, 22)) also showed the highest expression in cerebellum and a higher expression than that in linear form (Fig. 3M). We also observed that some loci generated multiple major circRNA transcripts, such as *Anks1b* and *Rere* (Fig. 3K and Supplementary file 1: Fig. S2). Unlike *Rims2*-dervied circRNAs, most *Rere*-dervied circRNAs showed a higher

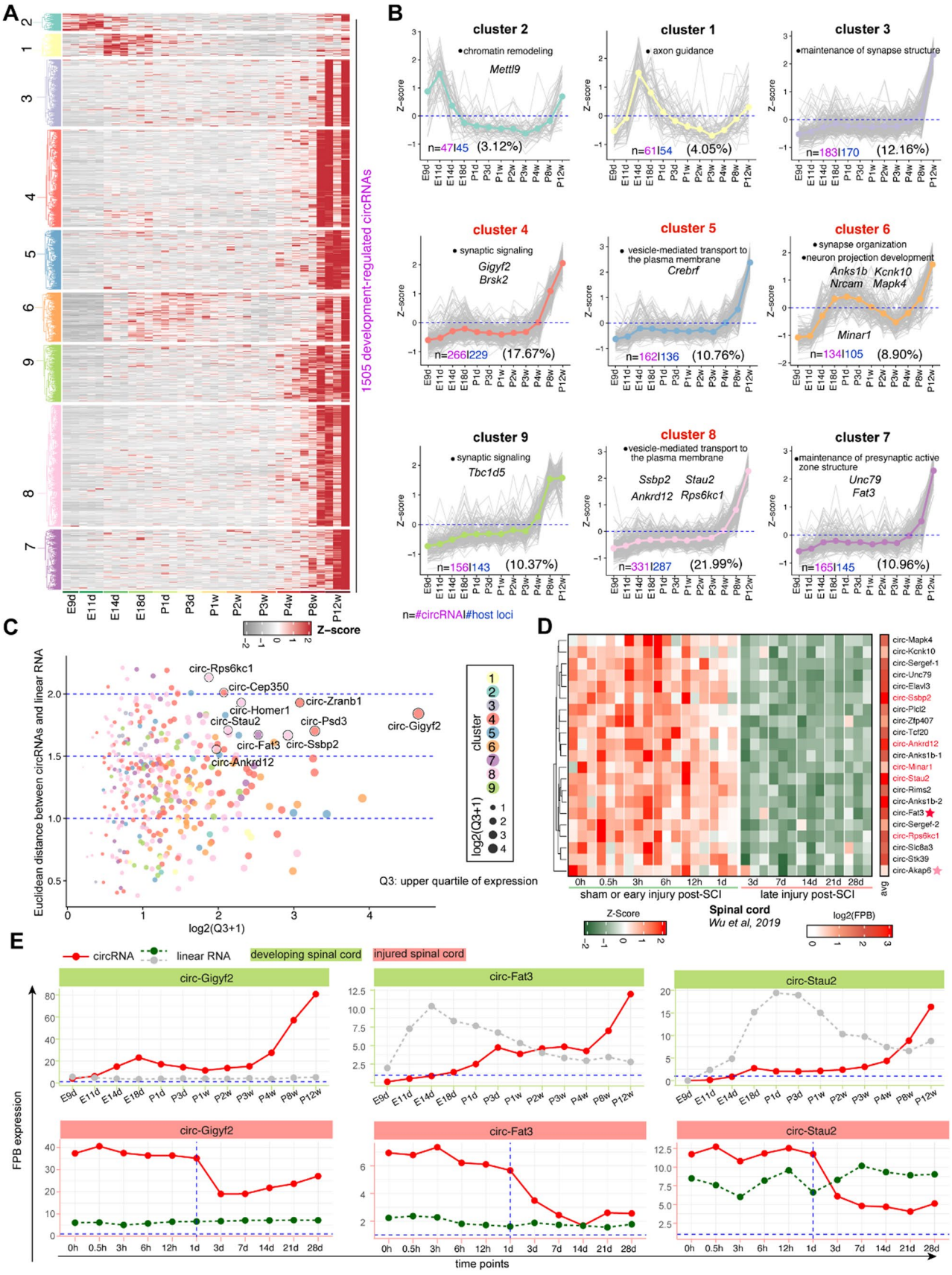
A
1505 development-regulated circRNAs
E9d E11d E14d E18d P1d P3d P1w P2w P3w P4w P8w P12w
Z-score
B
cluster 2
•chromatin remodeling
Mettl9
n=47|45 (3.12%)
cluster 1
• axon guidance
n=61|54 (4.05%)
cluster 3
•maintenance of synapse structure
n=183|170 (12.16%)
cluster 4
• synaptic signaling
Gigyf2
Brsk2
n=266|229 (17.67%)
cluster 5
• vesicle-mediated transport to the plasma membrane
Crebrf
n=162|136 (10.76%)
cluster 6
• synapse organization
•neuron projection development
Anks1b Kcnk10
Nrcam Mapk4
Minar1
n=134|105 (8.90%)
cluster 9
• synaptic signaling
Tbc1d5
n=156|143 (10.37%)
cluster 8
•vesicle-mediated transport to the plasma membrane
Ssbp2 Stau2
Ankrd12 Rps6kc1
n=331|287 (21.99%)
cluster 7
•maintenance of presynaptic active zone structure
Unc79
Fat3
n=165|145 (10.96%)
n=#circRNA|#host loci
C
Euclidean distance between circRNAs and linear RNA
log2(Q3+1)
circ-Rps6kc1
circ-Cep350
circ-Zranb1
circ-Homer1
circ-Stau2
circ-Psd3
circ-Gigyf2
circ-Fat3
circ-Ssbp2
circ-Ankrd12
cluster
log2(Q3+1)
Q3: upper quartile of expression
D
circ-Mapk4
circ-Kcnk10
circ-Sergef-1
circ-Unc79
circ-Elavl3
circ-Ssbp2
circ-Picl2
circ-Zfp407
circ-Tcf20
circ-Ankrd12
circ-Anks1b-1
circ-Minar1
circ-Stau2
circ-Rims2
circ-Anks1b-2
circ-Fat3
circ-Sergef-2
circ-Rps6kc1
circ-Slc8a3
circ-Stk39
circ-Akap6
avg
0h 0.5h 3h 6h 12h 1d 3d 7d 14d 21d 28d
sham or eary injury post-SCI
late injury post-SCI
Z-Score
Spinal cord
Wu et al, 2019
log2(FPB)
E
circRNA
linear RNA
developing spinal cord
injured spinal cord
circ-Gigyf2
circ-Fat3
circ-Stau2
FPB expression
time points

◂**Fig. 4** Expression patterns of circRNAs in developing and injured spinal cord and divergence between circRNAs and linear RNAs. **A** The expression of developmentally regulated circRNAs. **B** Expression patterns of circRNAs and enrichment terms of related host loci. **C** The expression divergence between circRNAs and linear RNAs. Point colors depict clusters in A and B panels. Point sizes depict upper quartile of expression abundance. **D** Expression patterns of 20 abundant circRNAs in spinal cord after injury (identified injury-related circRNAs were shown in Supplementary file 1: Fig. S9). "Avg" panel depict average of expression abundance. Pink star indicated validated expression in spinal cord after injury. Red star indicated documented exploration of function. **E** Three examples of circRNAs with expression diverged from that in linear RNAs during the developing and injured spinal cord

expression in cortex and multiple *Rere*-dervied circRNAs also showed a higher expression than that in linear form especially in medulla (Fig. 3K). We next focused on those CNS-enriched circRNAs with a higher CIRCscore (> 1) and classified into three categories according to the percent of expression in CNS tissues compared to that in the total tissues (Fig. 3J). As observed, a higher percent of CNS expression of circular form than that in the linear form, such as a circRNA produced by a long non-coding RNA (ENSRNOG00000066491, here designed as lncRNA-66491, Fig. 3J). We also checked CIRCscore of mouse orthologs using a mouse body dataset[9] and some of them showed a higher expression and a higher CIRCscore in brain than that in other tissues, such as a circRNA generated from *Boc* (Fig. 3J). Taken together, we showed the CNS-enriched circRNAs as well as circRNAs enriched in other tissues in rat.

Developmental- and injured-regulated circRNAs in rat spinal cord

After discussing circRNA expression in diverse tissues, we explored the changes in expression during central nervous system development and disease in rats. Due to a lack of long-term time-series RNA-Seq dataset for other rat CNS tissues, we used our developing spinal cord as well as injured spinal cord to investigate expression changes. First, we employed a regression-based method to detect significant expression profile difference of highly abundant circRNAs (BSJ read count ≥ 5 in at least two replicates) during the developing and injured spinal cord using the maSigPro package [21] respectively. We identified 1505 (out of 2289; 65.7%) developmental-regulated circRNAs generating from 979 loci and clustered into nine clusters (Fig. 4A and B). CircRNAs in most clusters presented a high expression in adult (P8w-P12w), except for the clusters 1 and 2. Functional enrichment of host loci generating circRNAs in clusters 1 and 2 were most enriched in the terms of "chromatin remodeling" and "axon guidance" respectively (Fig. 4B). A conserved circRNA (circ-*Mettl9*) from the cluster 2 with expression decrease along the development had been validated in mouse retinal development [13]. Host loci generating circRNAs in other clusters were most enriched in synapse or vesicle-mediated transport to the plasma membrane (Fig. 4B). Of other clusters, we noticed that circRNAs in the cluster 6 featured an increase at the neonatal stages (E18d ~ P3d) and parent host loci enriched in terms of "synapse organization" and "neuron projection development", including *Anks1b*, *Kcnk10*, *Nrcam*, *Mapk4*, and *Minar1* (Fig. 4B). Most abundant circRNAs were presented in the clusters 4 (*e.g.*, circ-*Gigyf2*), 5 (*e.g.*, circ-*Crebrf*) and 8 (*e.g.*, circ-*Ssbp2*). Several studies have described a low correlation between circRNA and cognate linear RNA forms [29]. It was also consistent that a low correlation (rho: 0.13) between circRNAs and cognate linear RNA forms using the expression abundance from this dataset of developing rat spinal cord (Supplementary file 1: Fig. S8). We next asked which circRNAs showed a large difference between circRNAs and cognate linear RNA forms. We then calculated Euclidean distance between circRNAs and linear RNA forms and also considered the abundance of circRNAs and presented in Fig. 4C. We found several top abundant circRNAs that displayed a large divergence, including circ-*Gigyf2*, circ-*Zranb1*, circ-*Ssbp2*, circ-*Fat3*, and circ-*Stau2* (Fig. 4C). Whether this characteristic also present using the dataset of injured spinal cord? We detected 240 injured-regulated circRNAs in long-term time-series of injured spinal cord (0.5 h (h) to 28 days post-injury, only rostral samples were considered). Most circRNAs were down-regulated, including circ-*Gigyf2*, circ-*Fat3*, and circ-*Stau2* (Fig. 4D and Supplementary file 1: Fig. S9). The expression patterns and validation of circRNAs (*e.g.*, circ-*Akap6*) have been described and validated in original publication of injured spinal cord [33]. Consistent observation in developing spinal cord, we also found some of those top abundant circRNAs (*e.g.*, circ-*Gigyf2*, circ-*Fat3*, circ-*Stau2* in Fig. 4E) showed divergent expression between circRNAs and cognate linear RNA forms after injury. For example, linear *Gigfy2* showed a little change in expression pattern during the developing and injured rat spinal cord, while circ-*Gigyf2* showed a dramatic increase in adult spinal cord and down-regulated after SCI (Fig. 4E). Taken together, we displayed the circRNAs expression patterns in rat spinal cord during the development and injury.

Experimental validation of circular RNAs in developing spinal cord and other tissues

We screened 12 circRNAs for experimental verification based on their abundance and expression changes across various tissues and during spinal cord development, including circRNAs derived from *Ssbp2* and *Minar1*. To verify the circular structure of these circRNAs, total RNA isolated from rat spinal cord was treated with RNase R, an exonuclease that selectively degrades linear RNAs. Following RNase

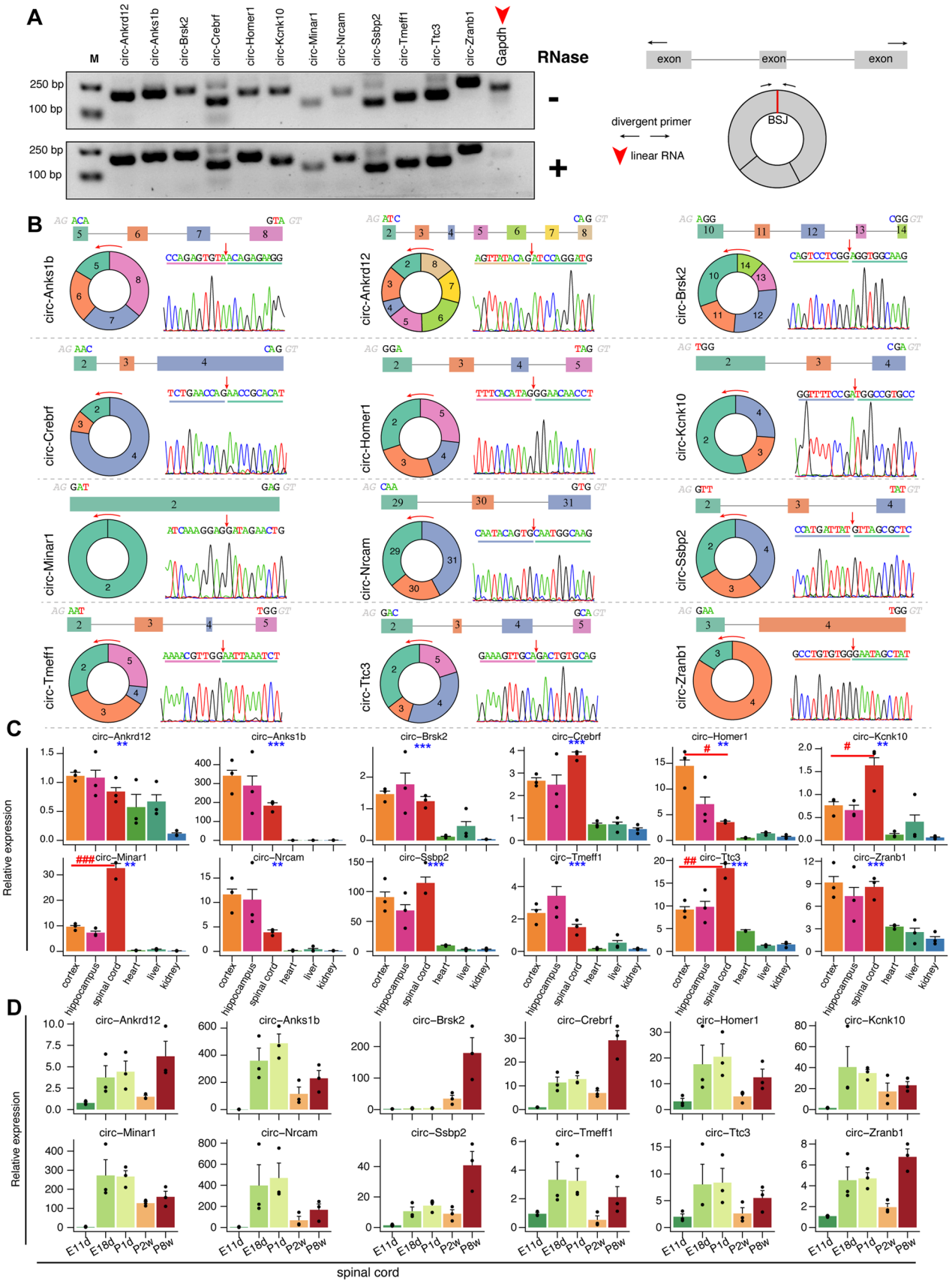
A
M
circ-Ankrd12
circ-Anks1b
circ-Brsk2
circ-Crebrf
circ-Homer1
circ-Kcnk10
circ-Minar1
circ-Nrcam
circ-Ssbp2
circ-Tmeff1
circ-Ttc3
circ-Zranb1
Gapdh
RNase
250 bp
100 bp
-
+
exon
divergent primer
linear RNA
BSJ
B
C
Relative expression
cortex
hippocampus
spinal cord
heart
liver
kidney
D
E11d
E18d
P1d
P2w
P8w
spinal cord

◂**Fig. 5** Experimental validation of 12 circRNAs and relative expression in diverse rat tissues and developing spinal cord. **A** Agarose gel electrophoresis assay confirmed the resistance to exonucleases of 12 candidate circRNAs by RNase R treatment. Linear *Gapdh* was used as the negative control. The uncropped electrophoresis image was shown in Supplementary file 1: Fig. S11. **B** Sanger sequencing result of qPCR products confirmed the back-splicing junction sequences from 12 candidate circRNAs. Arrows in the upper of base sequences indicated the back-splicing site. **C** Relative expression of 12 candidate circRNAs in six tissues of rats. Data are present as mean + S.E.M. (n = 3 samples per group, *p < 0.05, unpaired t-test; #p < 0.05, one-way ANOVA test). **D** Relative expression of 12 candidate circRNAs in five developmental timepoints of rat spinal cord. Data are present as mean + S.E.M. (n = 3 samples per group)

R treatment, PCR amplification using divergent primers, followed by agarose gel electrophoresis, yielded a detectable product specific to the circRNA (Fig. 5A). In contrast, the linear RNA (*Gapdh*) was vanished in the RNase R-treated sample, supporting the circular nature of the circRNAs. Subsequent Sanger sequencing of the PCR products confirmed the presence of the back-splicing junction (Fig. 5B), providing further evidence for the circular configuration of circRNAs. The above results validate the 12 circRNAs screened from the RNA sequencing datasets by RNase R treatment and Subsequent Sanger sequencing.

To assess the relative expression of these circRNAs, we conducted a qPCR experiment across six tissues (cortex, hippocampus, spinal cord, heart, liver, kidney) and five developmental timepoints (E11d, E18d, P1d, P2w, P8w) (Fig. 5C and 5D). All of these circRNAs exhibited significantly higher expression levels in CNS tissues (cortex, hippocampus, and spinal cord) compared to non-CNS tissues (heart, liver, kidney), such as circ-Anks1b, circ-Nrcam, circ-Minar1, and circ-Ssbp2 (Fig. 5C, $p < 0.05$, unpaired t-test). In addition, four circRNAs showed significantly differential expression across CNS tissues (Fig. 5C, $p < 0.05$, one-way ANOVA test). For example, circ-Minar1, consisting of a single exon, showed the highest expression in the rat spinal cord and was also highly expressed in the mouse spinal cord (Supplementary file 1: Fig. S10). Generally, these circRNAs had low expression at the early embryonic stage (E11d) and increased during later embryonic and neonatal stages (E18d and P1d), except for circ-Brsk2, which expressed only after adolescence (P2w) and increased with development. In summary, our experimental validation confirmed the circRNAs predicted from RNA sequencing datasets and their generally consistent expression patterns across tissues and developmental stages.

Functional exploration of abundant circRNAs in rat model

After confirming the accuracy of circRNA predictions, we explored their potential functions by integrating other omics datasets and bioinformatic predictions. The circRNAs function in various biological processes, including acting as sponges for miRNAs or RNA-binding proteins (RBPs) and translating into peptides or proteins [8]. We used ribosome footprint profiling (RFP), polysome profiling, and mass spectrometry to investigate the translation potential of circRNAs. Due to short fragment lengths in RFP (28–35 nt), translated circRNAs are often underestimated [11, 37]. We re-analyzed ribosome footprint and polysome profiling data from rat hippocampus [38]. As expected, no ribosome-associated circRNAs were detected in the RFP datasets using the same pipeline. However, we identified 8350 credible circRNAs (BSJ read count ≥ 5 in both two replicates), with 8280 (99.16%) in ribosome-free, 1186 (14.28%) in monosome-associated, and 123 (1.47%) in polysome-associated fractions (Fig. 6A). The ratio of expression between monosome- and polysome-associated circRNAs was higher for circRNAs and lower for linear RNAs (Fig. 6A), indicating that most circRNAs are not translated, and those that are tend to be associated more with monosomes [39]. We investigated the top 20 abundant polysome-associated circRNAs, including circ-Ssbp2, circ-Cdyl, circ-Nfix, and circ-Hipk3 (Fig. 6C and Fig. 6D). Most of these circRNAs were also highly abundant in the developing spinal cord, except for circRNAs from *Grm4* and *Boc* (Fig. 6C). Using IRESfinder and SRAMP, we predicted internal ribosomal entry sites (IRES) and N-6-methyladenosine (m6A) sites, finding that most of these circRNAs possessed open reading frames (ORF), IRES, and/or m6A sites (Fig. 6C), suggesting their potential for translation.

Next, we investigated the role of highly abundant circRNAs in the developing spinal cord as miRNA sponges. We considered only miRNAs with a maximum number of reads greater than 50 in at least two replicates (Fig. 1A). We scanned for miRNA binding sites spanning or near the back-splicing junction of circRNAs (pseudo-circRNAs) or within single-exon derived circRNAs. This analysis included 364 miRNAs and 2289 circRNAs (176 single-exon derived). We predicted 416 (194 miRNAs and 316 circRNAs) and 1522 (256 miRNAs and 167 circRNAs) miRNA-circRNA interactions for pseudo-circRNAs and single-exon derived circRNAs, respectively, with support from three tools (Supplementary file 4: Table S3).

We observed that miR-351-5p and miR-125a/b-5p may bind to circRNAs generated from *Coq3* (Coenzyme Q3, Fig. 6E). Among single-exon derived circRNAs, eight with a total BSJ read count greater than 1,000 had multiple miRNA binding sites, including circ-Fat3(2), circ-Slc8a1(2), and circ-Cdyl(2) (Fig. 6F). Circ-Fat3(2), generated from exon 2 of rat *Fat3* loci (orthologous to "mmu_circ_0001746" in mouse), is evolutionarily conserved and has been implicated in neural development in mice[40]. We predicted 25 miRNAs targeting circ-Fat3(2),

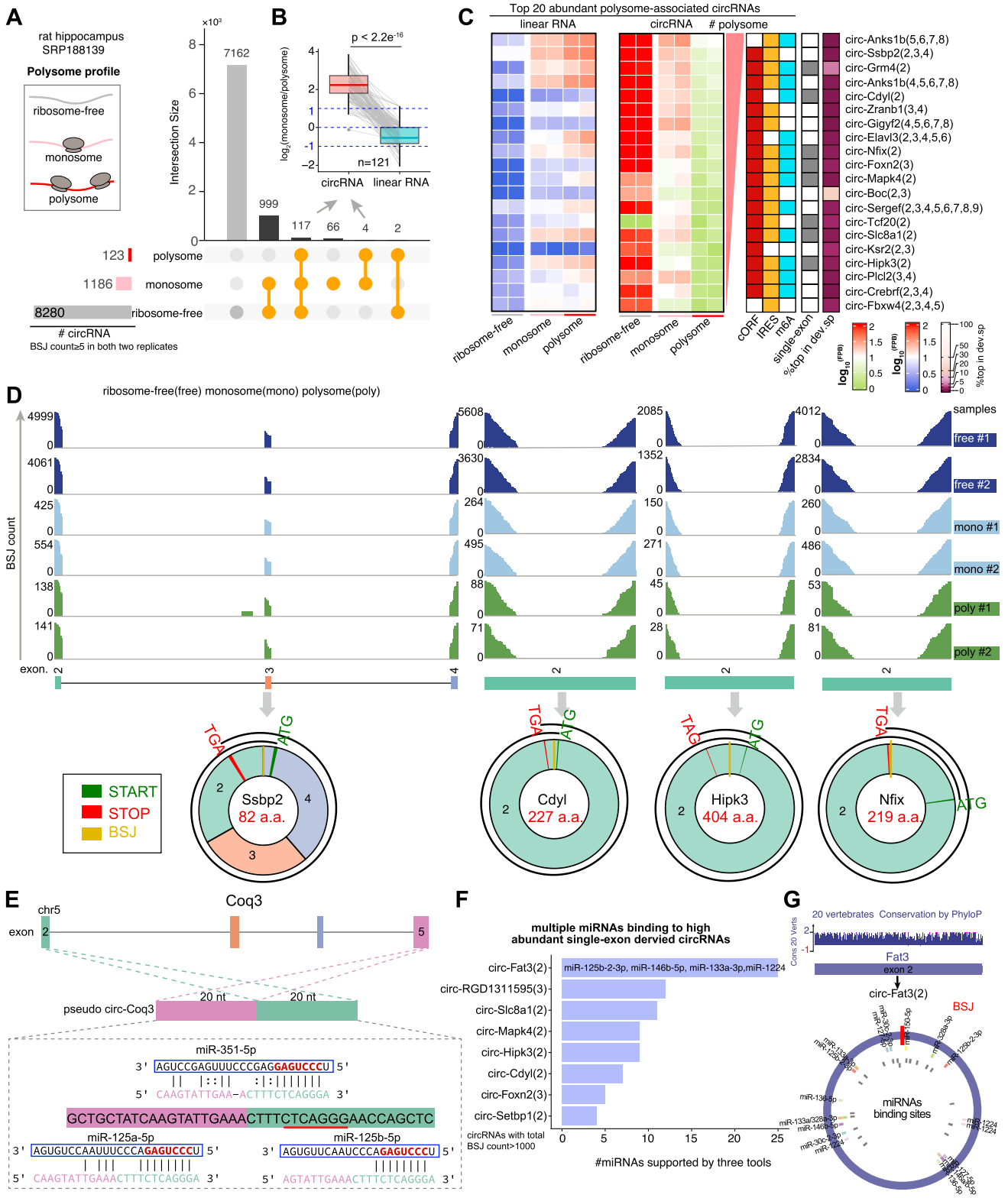

supported by three miRNA target prediction tools, including miR-125b-2-3p, miR-146b-5p, miR-133a-3p, and miR-1224 (Fig. 6F and Fig. 6G). These analyses suggest that circRNAs may act as miRNA sponges and potential

◂**Fig. 6** Functional exploration of candidate circRNAs by integrating multi-omics datasets and in silico. **A** The summary of the number of circRNAs identified from polysome profiling dataset of rat hippocampus. **B** The ratio between monosome- and polysome- expression in circRNAs and cognate linear RNAs. **C** The expression of top 20 polysome-associated circRNAs. **D** The BSJ coverage of four circRNAs as well as predicted the longest translated protein. **E** Three miRNAs may bind to the pseudo circ-*Coq3*. **F** High abundant single-exon derived circRNAs with multiple miRNAs binding. **G** The conserved circ-*Fat3*(2) and predicted miRNA binding sites. Colorful rectangles showed the top 10 abundant miRNAs, and grey rectangles showed other miRNA binding sites. The top 10 abundant miRNAs were labelled

translational templates, highlighting their diverse roles in gene regulation.

Overview of analyzed datasets and accessible resource

Overall, we re-analyzed a total of 22 RNA-Seq datasets from 20 publications[9–13, 15, 18, 28, 32, 34, 38, 41–49] with 15 (217 samples) from rat and 7 (94 samples) from mouse to reveal circular RNA repertoires in the developing spinal cord as well as in other tissues (Fig. 7A and Supplementary file 2: Table S1). For the investigation of circRNAs expression in tissues, we included two large body atlases for rat (SRP410543, 38 tissues, including different brain regions and spinal cord) and mouse (CRA000348, 14 tissues, including brain and spinal cord). For the investigation of circRNAs expression in CNS development, we included RNA-Seq datasets from the developing rat spinal cord, and brain and retina from mouse. We also included several RNA-Seq datasets from neuronal tissues under the condition of injury, such as spinal cord injury (SCI) and sciatic nerve crush (SNC) and ischemic injury. Most of these datasets were paired-end mode and the sequencing read length were 75–150 bp. We identified at least 15,251 reliable circRNAs from rat datasets and 34,396 circRNAs from mouse datasets (only BSJ read count ≥ 5 was counted) respectively. Due to the alternative splicing and short-read length of RNA-Seq, most tools identifying circRNAs depend on the detection of BSJ sites [50] that makes the number of predicted circRNAs is under-estimated and the structure is not full-length. To further explore circRNA function, we analyzed a polysome profiling of rat hippocampus and miRNA-Seq from rat spinal cord as well as bioinformatic prediction. Finally, we developed an online R shiny application (**Ci**rcular **RN**ome in R**at**, abbreviated as "*CiRNat*", http://121.41.67.1:3838/CiRNat/) for publicly accessible to this integrated resource (Fig. 7B). *CiRNat* has two main functional modules (browser and query) that enables users to explore and visualize the circular RNA information (*e.g.*, host loci, expression in distinct datasets, corresponding accession in the circAtlas) and expression abundance in different analyzed datasets.

Discussion

In this study, we characterized circular RNAs (circRNAs) in the developing rat spinal cord and conducted an integrated analysis incorporating additional relevant public RNA-Seq datasets, including whole-body organ atlases from both rat and mouse. Furthermore, we systematically compared circRNAs in central nervous system (CNS) and peripheral nervous system (PNS) tissues, and experimentally validated the expression and predicted results for 12 circRNAs through RNase R digestion, electrophoresis assay, and Sanger sequencing. These experimental results confirmed the high accuracy of circRNA prediction by CIRCexplore3 [19, 50].

Our findings demonstrate that the characteristics of circRNA expression in the analyzed rat datasets are highly consistent with previous studies [11, 29]. These features include low expression levels of circRNAs, enrichment of circRNAs derived from synapse-related protein-coding genes, high abundance in the brain—particularly in the cerebellum region, gradual upregulation during development, and low correlation with the expression of their linear RNA forms [10, 11, 51]. Previous studies on developing mouse brain and retina (E18d, P1d, P10d, P30d, etc.) have also shown consistent circRNA upregulation along the development process [11–13]. In contrast, we found that circRNAs are lowly expressed in the early embryonic stages (E9d and E11d) in rat spinal cord but increase significantly at E14d. This suggests two expression peaks in spinal cord development, closely associated with key developmental events such as the rapid growth of the nervous system, neural tube closure, and accelerated neuron differentiation [18].

Unlike the general upregulation of circRNAs observed during spinal cord development, we noticed that most differentially expressed circRNAs are downregulated in spinal cord injury (SCI), including the most abundant circ-Gigfy2. Gigfy2 linear mRNA encodes an essential RNA-binding protein involved in translation and is associated with psychiatric disorders such as schizophrenia and autism spectrum disorder [52, 53]. A search of mammalian organ development expression profiles revealed that the linear form of *Gigyf2* shows minimal expression changes across tissues, with a significant upregulation observed only in the testes during adulthood. However, the circRNA form of *Gigyf2* exhibits higher expression in CNS tissues compared to other tissues, including PNS tissues. As one of the most abundant circRNAs, although circ-Gigyf2 has been reported to be abundant in the mouse synapse, with in situ hybridization experiments showing localization in the cell body and dendrites of cultured mouse hippocampal neurons [11], its function remains to be further explored.

By analyzing RNA-Seq datasets from rat and mouse, we observed that the number of circRNAs detected in mice

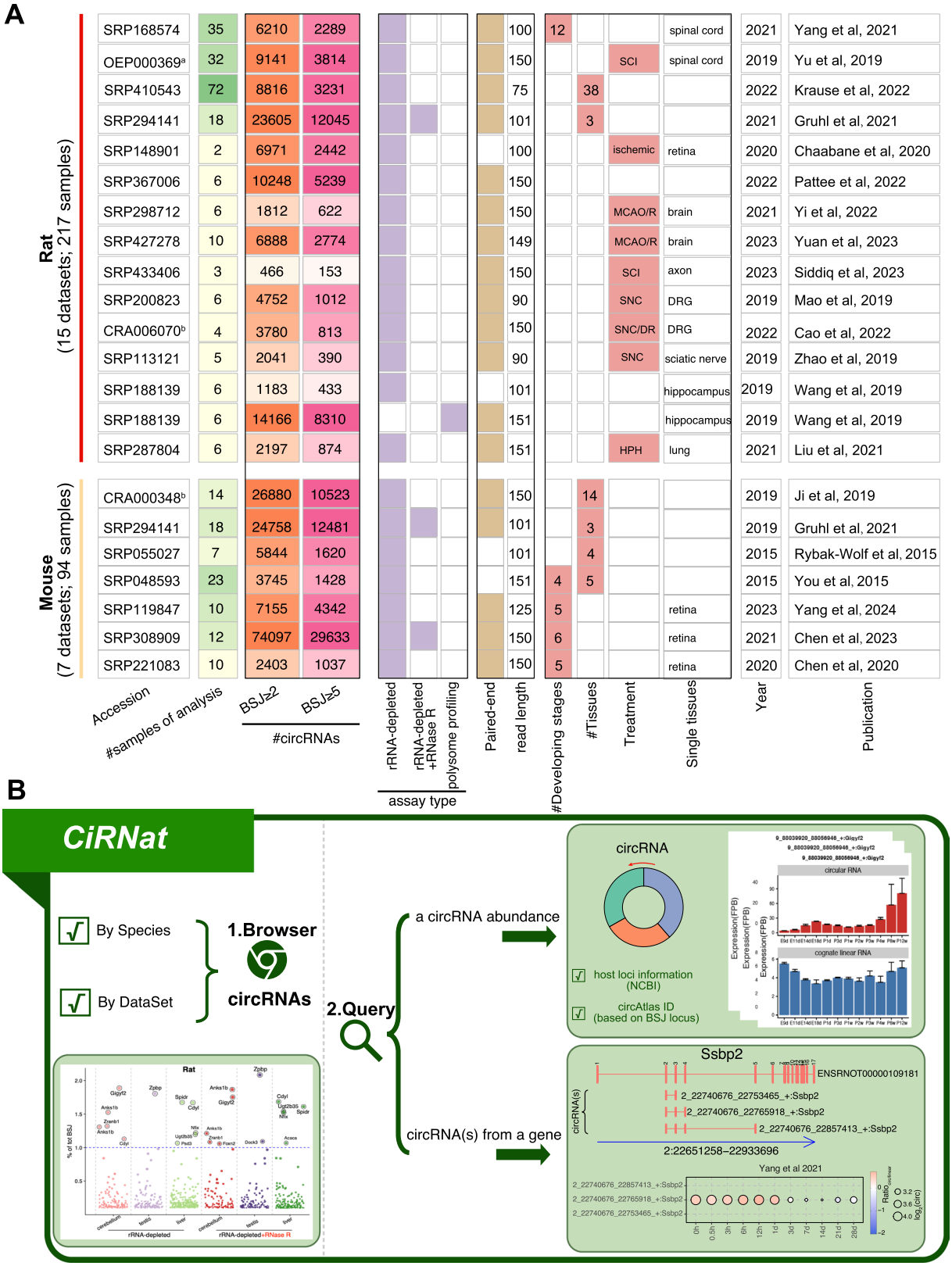

Fig. 7 Overview of the analyzed datasets and accessible resource. **A** Information of analyzed datasets, including species, accessions, number of samples, sequencing strategy, publication, and number of the circRNAs. **B** Main functional modules of the shiny application to access the data analyzed in this study, *CiRNat* (**Ci**rcular **RN**ome in **Rat**)

exceeds that in rats, with tissue-specific, highly abundant circRNAs showing notable differences between these species, particularly in the testes. This phenomenon may be attributed to differences in splicing factors and regulatory elements across species, which affect circRNA biogenesis efficiency and expression profiles [54–56]. The higher number of circRNAs detected in mice compared to rats is likely due to differences in genome annotation completeness, which affects the identification and cataloging of circRNAs across species. Similarly, distinct functional demands and gene expression requirements between tissues also lead to differential circRNA expression. Certain tissues, such as the testes, may require more circRNAs to regulate specific physiological processes, such as spermatogenesis [57–59].

While the function of circRNAs as miRNA sponges has been widely studied, only a handful of circRNAs have been validated to possess translational potential [6, 60]. Our reanalysis of previous polysome data revealed that most circRNAs could not be translated, with only a few circRNAs with potential open reading frames (ORFs) and internal ribosomal entry sites (IRES) showing translational potential, such as circ-Ssbp2, circ-Cdyl, and circ-Nfix. The translation products of these circRNAs could have significant biological implications in maintaining genomic stability, gene regulation, development, and physiological functions [61–63]. In recent years, circRNAs have been increasingly recognized for their roles in various diseases [64] particularly cancer and neurodegenerative disorders [51, 65, 66]. Some circRNAs, due to their stable circular structure, are considered promising as early biomarkers [67]. For example, certain circRNAs are overexpressed in cancer cells and may regulate pathways related to cell proliferation, making them potential targets for anticancer therapies [68]. Additionally, circRNAs have shown potential in neurodegenerative diseases, where their roles in neuronal homeostasis and synaptic function may provide new insights into disease mechanisms [69, 70]. Emerging technologies like single-cell sequencing and spatial transcriptomics provide valuable tools for investigating circRNA functions at cell-type and tissue-specific levels [71], enhancing our understanding of their roles in cellular differentiation, tissue structure, and CNS mechanisms [72].

This study also has certain limitations. First, our research relies heavily on publicly available RNA-Seq datasets, which vary in quality and sequencing depth. These variations can introduce bias in circRNA identification, potentially leading to an underrepresentation of low-abundance circRNAs. For instance, limited sequencing depth in some datasets may fail to capture the full circRNA repertoire, particularly for circRNAs with lower expression levels. Another potential source of bias arises from differences in genome annotation completeness. Since the rat genome is currently less comprehensively annotated than the mouse genome, certain circRNA detection algorithms that heavily rely on genome annotation completeness, such as CIRCexplore3, may introduce additional bias due to their underlying computational methods, leading to lower circRNA counts in rat datasets. Future research could address this limitation by enhancing genome annotation through large-scale RNA-Seq data integration and advanced circRNA prediction tools. Lastly, while we performed experimental validation on a subset of 12 circRNAs, this relatively small sample size may limit the generalizability of our findings to all identified circRNAs, and more extensive validation across different developmental stages and tissue types is essential to fully understand circRNAs' functional roles. Gene-editing tools like CRISPR/Cas9, along with single-cell sequencing and spatial transcriptomics, will be essential for exploring the functions of key circRNAs and evaluating their potential as biomarkers or therapeutic targets [73].

In conclusion, this research presents the first comprehensive landscape of circRNAs across various rat tissues, emphasizing spinal cord development and injury responses. Our findings reveal distinct circRNA expression patterns that may enhance understanding of their roles in neural development and pathology. This resource provides a valuable foundation for exploring circRNA functions and holds promise for identifying biomarkers or therapeutic targets in neurobiology and clinical research, potentially advancing diagnostic and treatment approaches for neurological disorders.

Supplementary Information The online version contains supplementary material available at https://doi.org/10.1007/s00018-025-05665-1.

Author contributions L.X., J.Y., Z.M.C. and X.S.G. designed the experiments. L.X. and J.Y. performed data collections and pre-processing. J.Y., and L.X. analyzed the whole analysis. N.N.J., S.Q.Z., Y.T. and J.Y. performed the experimental validation. J.Y. and L.X. wrote the draft manuscript. N.N.J., Z.M.C., and X.S.G. revised the manuscript. Z.M.C., J.H.S., B.Y., G.C.L., X.L.H. and Z.F.C provide technical assistance with data collection and analysis and joined the discussion.

Funding Qinglan Project of Jiangsu Province of China, 2024, Guicai Li, National Natural Science Foundation of China, 32130060, Xiaosong Gu, 82171425, Nana Jin, 32171352, Guicai Li, Natural Science Foundation of Jiangsu Province, BK20232023, Xiaosong Gu, Nantong University Talent Cultivation Support Project, 135424624019, Jian Yang.

Data availability All datasets analyzed in this study were retrieved from the public databases (SRA or National Genomics Data Center or NODE) under accessions (Supplementary file 2: Table S1 and Supplementary file 3: Table S2). CircRNA annotation and expression abundance identified from the analyzed datasets using the universal pipeline, source code for the *CiRNat* shiny application (http://121.41.67.1:3838/CiRNat/) have been deposited in the figshare database (DOI:10.6084/m9.figshare.25952245v1). The source code employed in this study is accessible on Figshare at the following repository: https://figshare.com/articles/software/CiRNat_tar_gz/25952245.

Declarations

Conflict of interests The authors declare no potential competing interests.

Ethical approval and consent to participate This study was conducted in strict accordance with the ethical standards and guidelines of the Nantong University Institutional Animal Care and Use Committee.

Consent for publication All authors agree with the publication of this article.

Open Access This article is licensed under a Creative Commons Attribution-NonCommercial-NoDerivatives 4.0 International License, which permits any non-commercial use, sharing, distribution and reproduction in any medium or format, as long as you give appropriate credit to the original author(s) and the source, provide a link to the Creative Commons licence, and indicate if you modified the licensed material. You do not have permission under this licence to share adapted material derived from this article or parts of it. The images or other third party material in this article are included in the article's Creative Commons licence, unless indicated otherwise in a credit line to the material. If material is not included in the article's Creative Commons licence and your intended use is not permitted by statutory regulation or exceeds the permitted use, you will need to obtain permission directly from the copyright holder. To view a copy of this licence, visit http://creativecommons.org/licenses/by-nc-nd/4.0/.

References

1. Dong X, Bai Y, Liao Z, Gritsch D, Liu X, Wang T, Borges-Monroy R, Ehrlich A, Serrano GE, Feany MB et al (2023) Circular RNAs in the human brain are tailored to neuron identity and neuropsychiatric disease. Nat Commun 14:5327
2. Mehta SL, Dempsey RJ, Vemuganti R (2020) Role of circular RNAs in brain development and CNS diseases. Prog Neurobiol 186:101746
3. Liu W, Liang W, Xiong XP, Li JL, Zhou R (2022) A circular RNA Edis-Relish-castor axis regulates neuronal development in Drosophila. PLoS Genet 18:e1010433
4. Kristensen LS, Jakobsen T, Hager H, Kjems J (2022) The emerging roles of circRNAs in cancer and oncology. Nat Rev Clin Oncol 19:188–206
5. Memczak S, Jens M, Elefsinioti A, Torti F, Krueger J, Rybak A, Maier L, Mackowiak SD, Gregersen LH, Munschauer M et al (2013) Circular RNAs are a large class of animal RNAs with regulatory potency. Nature 495:333–338
6. Pamudurti NR, Bartok O, Jens M, Ashwal-Fluss R, Stottmeister C, Ruhe L, Hanan M, Wyler E, Perez-Hernandez D, Ramberger E et al (2017) Translation of CircRNAs. Mol Cell 66(9–21):e27
7. Chen R, Yang T, Jin B, Xu W, Yan Y, Wood N, Lehmann HI, Wang S, Zhu X, Yuan W et al (2023) CircTmeff1 promotes muscle atrophy by interacting with TDP-43 and encoding a novel TMEFF1-339aa protein. Adv Sci (Weinh) 10:e2206732
8. Chen LL (2020) The expanding regulatory mechanisms and cellular functions of circular RNAs. Nat Rev Mol Cell Biol 21:475–490
9. Ji P, Wu W, Chen S, Zheng Y, Zhou L, Zhang J, Cheng H, Yan J, Zhang S, Yang P, Zhao F (2019) Expanded expression landscape and prioritization of circular rnas in mammals. Cell Rep 26(3444–3460):e3445
10. Rybak-Wolf A, Stottmeister C, Glazar P, Jens M, Pino N, Giusti S, Hanan M, Behm M, Bartok O, Ashwal-Fluss R et al (2015) Circular RNAs in the mammalian brain are highly abundant, conserved, and dynamically expressed. Mol Cell 58:870–885
11. You X, Vlatkovic I, Babic A, Will T, Epstein I, Tushev G, Akbalik G, Wang M, Glock C, Quedenau C et al (2015) Neural circular RNAs are derived from synaptic genes and regulated by development and plasticity. Nat Neurosci 18:603–610
12. Chen G, Qian HM, Chen J, Wang J, Guan JT, Chi ZL (2021) Whole transcriptome sequencing identifies key circRNAs, lncRNAs, and miRNAs regulating neurogenesis in developing mouse retina. BMC Genomics 22:779
13. Chen XJ, Zhang ZC, Wang XY, Zhao HQ, Li ML, Ma Y, Ji YY, Zhang CJ, Wu KC, Xiang L et al (2020) The circular RNome of developmental retina in mice. Mol Ther Nucleic Acids 19:339–349
14. Ahuja CS, Wilson JR, Nori S, Kotter MRN, Druschel C, Curt A, Fehlings MG (2017) Traumatic spinal cord injury. Nat Rev Dis Primers 3:17018
15. Yu B, Yao C, Wang Y, Mao S, Wang Y, Wu R, Feng W, Chen Y, Yang J, Xue C et al (2019) The landscape of gene expression and molecular regulation following spinal cord Hemisection in rats. Front Mol Neurosci 12:287
16. Chen S, Zhou Y, Chen Y, Gu J (2018) fastp: an ultra-fast all-in-one FASTQ preprocessor. Bioinformatics 34:i884–i890
17. Langmead B, Salzberg SL (2012) Fast gapped-read alignment with Bowtie 2. Nat Methods 9:357–359
18. Yang J, Zhao L, Yi S, Ding F, Yang Y, Liu Y, Wang Y, Liu M, Xue C, Xu L et al (2021) Developmental temporal patterns and molecular network features in the transcriptome of rat spinal cord. Engineering 7:1592–1602
19. Ma XK, Wang MR, Liu CX, Dong R, Carmichael GG, Chen LL, Yang L (2019) CIRCexplorer3: A CLEAR pipeline for direct comparison of circular and linear RNA expression. Genomics Proteomics Bioinformatics 17:511–521
20. Wu W, Zhao F, Zhang J (2023) circAtlas 3.0: a gateway to 3 million curated vertebrate circular RNAs based on a standardized nomenclature scheme. Nucleic Acids Res. https://doi.org/10.1093/nar/gkad770
21. Conesa A, Nueda MJ, Ferrer A, Talon M (2006) maSigPro: a method to identify significantly differential expression profiles in time-course microarray experiments. Bioinformatics 22:1096–1102
22. Fehlmann T, Kern F, Laham O, Backes C, Solomon J, Hirsch P, Volz C, Muller R, Keller A (2021) miRMaster 2.0: multi-species non-coding RNA sequencing analyses at scale. Nucleic Acids Res 49:W397–W408
23. Enright AJ, John B, Gaul U, Tuschl T, Sander C, Marks DS (2003) MicroRNA targets in Drosophila. Genome Biol 5:R1
24. Kertesz M, Iovino N, Unnerstall U, Gaul U, Segal E (2007) The role of site accessibility in microRNA target recognition. Nat Genet 39:1278–1284
25. Agarwal V, Bell GW, Nam JW, Bartel DP (2015) Predicting effective microRNA target sites in mammalian mRNAs. Elife. https://doi.org/10.7554/eLife.05005
26. Zhao J, Wu J, Xu T, Yang Q, He J, Song X (2018) IRESfinder: identifying RNA internal ribosome entry site in eukaryotic cell using framed k-mer features. J Genet Genomics 45:403–406
27. Zhou Y, Zeng P, Li YH, Zhang Z, Cui Q (2016) SRAMP: prediction of mammalian N6-methyladenosine (m6A) sites based on sequence-derived features. Nucleic Acids Res 44:e91
28. Gruhl F, Janich P, Kaessmann H, Gatfield D (2021) Circular RNA repertoires are associated with evolutionarily young transposable elements. Elife. https://doi.org/10.7554/eLife.67991
29. Vo JN, Cieslik M, Zhang Y, Shukla S, Xiao L, Zhang Y, Wu YM, Dhanasekaran SM, Engelke CG, Cao X et al (2019) The landscape of circular RNA in cancer. Cell 176(869–881):e813
30. Mahmoudi E, Cairns MJ (2019) Circular RNAs are temporospatially regulated throughout development and ageing in the rat. Sci Rep 9:2564

31. Zhou T, Xie X, Li M, Shi J, Zhou JJ, Knox KS, Wang T, Chen Q, Gu W (2018) Rat BodyMap transcriptomes reveal unique circular RNA features across tissue types and developmental stages. RNA 24:1443–1456
32. Krause C, Suwada K, Blomme EAG, Kowalkowski K, Liguori MJ, Mahalingaiah PK, Mittelstadt S, Peterson R, Rendino L, Vo A, Van Vleet TR (2022) Preclinical species gene expression database: development and meta-analysis. Front Genet 13:1078050
33. Wu R, Mao S, Wang Y, Zhou S, Liu Y, Liu M, Gu X, Yu B (2019) Differential circular RNA expression profiles following spinal cord injury in rats: a temporal and experimental analysis. Front Neurosci 13:1303
34. Cao HJ, Huang L, Zheng MR, Zhang T, Xu LC (2022) Characterization of circular RNAs in dorsal root ganglia after central and peripheral axon injuries. Front Cell Neurosci 16:1046050
35. Wang JJ, Shan K, Liu BH, Liu C, Zhou RM, Li XM, Dong R, Zhang SJ, Zhang SH, Wu JH, Yan B (2018) Targeting circular RNA-ZRANB1 for therapeutic intervention in retinal neurodegeneration. Cell Death Dis 9:540
36. Hansen TB, Jensen TI, Clausen BH, Bramsen JB, Finsen B, Damgaard CK, Kjems J (2013) Natural RNA circles function as efficient microRNA sponges. Nature 495:384–388
37. Ye Y, Wang Z, Yang Y (2021) Comprehensive identification of translatable circular RNAs using polysome profiling. Bio Protoc 11:e4167
38. Wang X, You X, Langer JD, Hou J, Rupprecht F, Vlatkovic I, Quedenau C, Tushev G, Epstein I, Schaefke B et al (2019) Full-length transcriptome reconstruction reveals a large diversity of RNA and protein isoforms in rat hippocampus. Nat Commun 10:5009
39. Yang Y, Fan X, Mao M, Song X, Wu P, Zhang Y, Jin Y, Yang Y, Chen LL, Wang Y et al (2017) Extensive translation of circular RNAs driven by N(6)-methyladenosine. Cell Res 27:626–641
40. Seeler S, Andersen MS, Sztanka-Toth T, Rybiczka-Tesulov M, van den Munkhof MH, Chang CC, Maimaitili M, Veno MT, Hansen TB, Pasterkamp RJ et al (2023) A circular RNA expressed from the FAT3 locus regulates neural development. Mol Neurobiol 60:3239–3260
41. Liu J, Deng Y, Fan Z, Xu S, Wei L, Huang X, Xing X, Yang J (2021) Construction and analysis of the abnormal lncRNA-miRNA-mRNA network in hypoxic pulmonary hypertension. Biosci Rep. https://doi.org/10.1042/BSR20210021
42. Zhao L, Yi S (2019) Transcriptional landscape of alternative splicing during peripheral nerve injury. J Cell Physiol 234:6876–6885
43. Mao S, Huang T, Chen Y, Shen L, Zhou S, Zhang S, Yu B (2019) Circ-Spidr enhances axon regeneration after peripheral nerve injury. Cell Death Dis 10:787
44. Siddiq MM, Toro CA, Johnson NP, Hansen J, Xiong Y, Mellado W, Tolentino RE, Johnson K, Jayaraman G, Suhail Z et al (2023) Spinal cord injury regulates circular RNA expression in axons. Front Mol Neurosci 16:1183315
45. Shan YUAN, YY, XU Meimei, HU Guangze, TANG Juan, GAO Rui, (2023) Structural variation and expression analysis of mRNAome and lncRNAome in cortex of rat middle cerebral artery occlusion model. J Shandong Univ (Health Sciences) 61:27–37
46. Yang L, Yi L, Yang J, Zhang R, Xie Z, Wang H (2024) Temporal landscape and translational regulation of A-to-I RNA editing in mouse retina development. BMC Biol 22:106
47. Chaabane M, Andreeva K, Hwang JY, Kook TL, Park JW, Cooper NGF (2020) seekCRIT: Detecting and characterizing differentially expressed circular RNAs using high-throughput sequencing data. PLoS Comput Biol 16:e1008338
48. Pattee J, Vanderlinden LA, Mahaffey S, Hoffman P, Tabakoff B, Saba LM (2022) Evaluation and characterization of expression quantitative trait analysis methods in the Hybrid Rat Diversity Panel. Front Genet 13:947423
49. Yi D, Wang Q, Zhao Y, Song Y, You H, Wang J, Liu R, Shi Z, Chen X, Luo Q (2021) Alteration of N (6)-methyladenosine mRNA methylation in a rat model of cerebral ischemia-reperfusion injury. Front Neurosci 15:605654
50. Vromman M, Anckaert J, Bortoluzzi S, Buratin A, Chen CY, Chu Q, Chuang TJ, Dehghannasiri R, Dieterich C, Dong X et al (2023) Large-scale benchmarking of circRNA detection tools reveals large differences in sensitivity but not in precision. Nat Methods 20:1159–1169
51. Xu K, Zhang Y, Li J (2021) Expression and function of circular RNAs in the mammalian brain. Cell Mol Life Sci 78:4189–4200
52. Thyme SB, Pieper LM, Li EH, Pandey S, Wang Y, Morris NS, Sha C, Choi JW, Herrera KJ, Soucy ER et al (2019) Phenotypic landscape of Schizophrenia-associated genes defines candidates and their shared functions. Cell 177(478–491):e420
53. Wang T, Guo H, Xiong B, Stessman HA, Wu H, Coe BP, Turner TN, Liu Y, Zhao W, Hoekzema K et al (2016) De novo genic mutations among a Chinese autism spectrum disorder cohort. Nat Commun 7:13316
54. Li S, Yang P (2021) Relationship between HSPA1A-regulated gene expression and alternative splicing in mouse cardiomyocytes and cardiac hypertrophy. J Thorac Dis 13:5517–5533
55. Montanes-Agudo P, Aufiero S, Schepers EN, van der Made I, Cocera-Ortega L, Ernault AC, Richard S, Kuster DWD, Christoffels VM, Pinto YM, Creemers EE (2023) The RNA-binding protein QKI governs a muscle-specific alternative splicing program that shapes the contractile function of cardiomyocytes. Cardiovasc Res 119:1161–1174
56. Short S, Peterkin T, Guille M, Patient R, Sharpe C (2015) Short linear motif acquisition, exon formation and alternative splicing determine a pathway to diversity for NCoR-family co-repressors. Open Biol. https://doi.org/10.1098/rsob.150063
57. Zhou F, Chen W, Jiang Y, He Z (2019) Regulation of long non-coding RNAs and circular RNAs in spermatogonial stem cells. Reproduction 158:R15–R25
58. Saberiyan M, Karimi E, Safi A, Movahhed P, Dehdehi L, Haririan N, Mirfakhraie R (2023) Circular RNAs: novel biomarkers in spermatogenesis defects and male infertility. Reprod Sci 30:62–71
59. Khan IM, Liu H, Zhuang J, Khan NM, Zhang D, Chen J, Xu T, Avalos LFC, Zhou X, Zhang Y (2021) Circular RNA expression and regulation profiling in testicular tissues of immature and mature Wandong Cattle (*Bos taurus*). Front Genet 12:685541
60. Wen SY, Qadir J, Yang BB (2022) Circular RNA translation: novel protein isoforms and clinical significance. Trends Mol Med 28:405–420
61. Wei Y, Chen X, Liang C, Ling Y, Yang X, Ye X, Zhang H, Yang P, Cui X, Ren Y et al (2020) A noncoding regulatory RNAs network driven by Circ-CDYL acts specifically in the early stages hepatocellular carcinoma. Hepatology 71:130–147
62. Liu Y, Liu S, Yuan S, Yu H, Zhang Y, Yang X, Xie G, Chen Z, Li W, Xu B et al (2017) Chromodomain protein CDYL is required for transmission/restoration of repressive histone marks. J Mol Cell Biol 9:178–194
63. Fraser J, Essebier A, Brown AS, Davila RA, Harkins D, Zalucki O, Shapiro LP, Penzes P, Wainwright BJ, Scott MP et al (2020) Common regulatory targets of NFIA, NFIX and NFIB during postnatal cerebellar development. Cerebellum 19:89–101
64. Fan W, Pang H, Xie Z, Huang G, Zhou Z (2022) Circular RNAs in diabetes mellitus and its complications. Front Endocrinol (Lausanne) 13:885650
65. D'Anca M, Buccellato FR, Fenoglio C, Galimberti D (2022) Circular RNAs: emblematic players of neurogenesis and neurodegeneration. Int J Mol Sci. https://doi.org/10.3390/ijms23084134

66. Vakili O, Asili P, Babaei Z, Mirahmad M, Keshavarzmotamed A, Asemi Z, Mafi A (2022) Circular RNAs in Alzheimer's disease: a new perspective of diagnostic and therapeutic targets. CNS Neurol Disord Drug Targets. https://doi.org/10.2174/1871527321666220829164211
67. Sarkar D, Diermeier SD (2021) Circular RNAs: potential applications as therapeutic targets and biomarkers in breast cancer. Noncoding RNA. https://doi.org/10.3390/ncrna7010002
68. Liccardo F, Iaiza A, Sniegocka M, Masciarelli S, Fazi F (2022) Circular RNAs activity in the leukemic bone marrow microenvironment. Noncoding RNA. https://doi.org/10.3390/ncrna8040050
69. Gu A, Jaijyan DK, Yang S, Zeng M, Pei S, Zhu H (2023) Functions of circular RNA in human diseases and illnesses. Noncoding RNA. https://doi.org/10.3390/ncrna9040038
70. Latowska J, Grabowska A, Zarebska Z, Kuczynski K, Kuczynska B, Rolle K (2020) Non-coding RNAs in brain tumors, the contribution of lncRNAs, circRNAs, and snoRNAs to cancer development-their diagnostic and therapeutic potential. Int J Mol Sci. https://doi.org/10.3390/ijms21197001
71. Gao X, Sun Z, Liu X, Luo J, Liang X, Wang H, Zhou J, Yang C, Wang T, Li J (2024) 127aa encoded by circSpdyA promotes FA synthesis and NK cell repression in breast cancers. Cell Death Differ. https://doi.org/10.1038/s41418-024-01396-1
72. Zhou Z, Zhang J, Zheng X, Pan Z, Zhao F, Gao Y (2024) CIRI-deep enables single-cell and spatial transcriptomic analysis of circular RNAs with deep learning. Adv Sci (Weinh) 11:e2308115
73. Wu W, Zhang J, Cao X, Cai Z, Zhao F (2022) Exploring the cellular landscape of circular RNAs using full-length single-cell RNA sequencing. Nat Commun 13:3242

Publisher's Note Springer Nature remains neutral with regard to jurisdictional claims in published maps and institutional affiliations.